High-precision Carrier Tracking Algorithm for extremely Weak and High-Dynamic Signal

Tao Deng[1,2], Maoli Ma[1], Qinghui Liu[1], Yajun Wu[1]

[1]Shanghai Astronomical Observatory, Chinese Academy of Sciences, Shanghai 200030, China
[2]University of Chinese Academy of Sciences, Beijing 100049, China

Key Points:

- Obtaining high-precision Doppler frequency for high-dynamic and very weak signals in deep space exploration is challenging.
- By replacing the arctangent phase detector with novel phase detector, the performances of PLL are greatly improved, including the high-dynamic and weak-signal tracking ability, tracking accuracy.
- The new proposed method is suitable for carrier tracking in deep space exploration, especially when large dynamic is contained in signals.

Corresponding author: Tao Deng; Qinghui Liu, dengtao@shao.ac.cn; liuqinghui@shao.ac.cn

Abstract

Obtaining high-precision Doppler frequency for very weak signals in deep space exploration is challenging. A phase-locked loop (PLL) is a widely used high-precision Doppler frequency measurement method, and the arctangent phase detector is the most widely used phase detector. However, the arctangent phase detector cannot correctly identify the signal phase for signals with very low signal-to-noise ratio (SNR) and very high dynamic. Therefore, the arctangent phase detector is the key module limiting the weak-signal and high-dynamic tracking abilities of a PLL. This study proposes a new phase discrimination method in which the phase difference between the real and the reconstructed signals is obtained by using the coefficients of signal transformation. By replacing arctangent phase detector with novel phase detector, the high-dynamic and weak-signal tracking abilities of PLL are greatly improved. This method is expected to provide a good reference for radar, navigation, and other fields involving carrier tracking, and it provides feasible technical solutions for high-precision carrier tracking of high-dynamic and low-SNR signals on some occasions.

1 Introduction

In deep space exploration, the signals received by ground stations are often very weak and contain a large dynamic Doppler effect. Consider the examples of the Mars Exploration Rover (MER) missions MER-A and MER-B : in the entry, descent, and landing (EDL) phase, the range of the first and second derivatives of the Doppler frequency is $0 \sim 1200Hz/s$ and around $-25Hz/s^2 \sim 40Hz/s^2$, respectively(Satorius et al., 2003). The first derivative of the Curiosity probe's Doppler frequency is even close to $3500Hz/s$(Soriano et al., 2012; Hao et al., 2018). At the same time, the signals received by the ground stations are very weak. For signals of the Curiosity probes EDL phase received by the 70-m antenna, the carrier-to-noise ratio (CNR) is around $27dB\text{-}Hz$ under normal conditions(Hao et al., 2018). During the Jupiter probe's Jupiter orbital insertion (JOI) phase, the CNR of the signal received by the ground station was as low as $12 \sim 15dB\text{-}Hz$(Soriano et al., 2012). These observations indicate that high-precision tracking of signals with very low signal-to-noise ratio (SNR) or high dynamic is one of the focal problems in communication for deep space exploration. This problem also applies to other application fields involving carrier tracking, such as a global navigation satellite system (GNSS) receiver: the satellite signal received by the receiver is very weak under the action of some natural or artificial factors. Therefore, it is also essential to develop a corresponding high-sensitivity and high-precision carrier tracking algorithm.

For estimating the Doppler frequency in Mars rover's EDL phase, one method compensated a series of phases for the original signal in the time domain and then detected the compensation value corresponding to the maximum energy to determine the Doppler frequency(Satorius et al., 2003). Maximum likelihood estimation is also a feasible method for carrier tracking in EDL phase(Cattivelli et al., 2008). However, the both methods are open-loop methods which require considerable computational resources to realize real-time processing, especially when sampling rate of data is large. Further, since only linear frequency model is considered, these two methods have limited tracking accuracy. Another study proposed an adaptive linear prediction method (ALP) to estimate the Doppler frequency(Lopes et al., 2006). Compared with the method proposed in(Satorius et al., 2003), ALP requires significantly lesser computational resources; however, its tracking accuracy remains inadequate.

A frequency-locked loop (FLL) based on a fast Fourier transform (FFT) frequency discriminator has a strong ability to track a weak signal. However, the FFT frequency discriminator has low frequency resolution, resulting in low tracking accuracy of Doppler frequency. Furthermore, the dynamic tracking ability is restricted by the characteristics of the FFT frequency discriminator itself.

A phase-locked loop (PLL) is a high-precision Doppler frequency tracking algorithm. Phase-locked loop (PLL) architectures are still widely used in many modern receivers. How-

ever, a traditional PLL is seriously compromised by many factors, including high dynamics, shadowing, strong fadings and so on(Vila-Valls et al., 2017).

Therefore, many PLL improvement strategies have been proposed. One is to combine the FLL with the PLL; doing so combines the high-dynamic tracking capability of the FLL with the high-precision tracking capability of the PLL(Mao & Chen, 2008). The tracking accuracy and weak-signal tracking ability of the PLL can also be improved by adopting Kalman filters (KF)(Won et al., 2012). Furthermore, adaptive KFs (AKFs) provide robust solutions compared with KFs(Vil-Valls et al., 2015; Won, 2014). It is also feasible to combine wavelet packet denoising with a PLL to improve the tracking accuracy or weak-signal tracking ability of a PLL(Li et al., 2011). In addition, discrete wavelet transform filtering and Kalman filters(KF) are combined to enhance signal carrier tracking robustness(Ruan et al., 2017).Wavelet de-noising adaptive Kalman filter (AKF) are also presented in Sun et al. (2017); Pengyue et al. (2016).

In this study, the phase discriminator is recognized as a key module that limits PLL performance improvement, and a new phase discriminator is designed by signal transformation which basis function is new defined. The novel phase detector is used to replace the traditional arctangent phase detector, resulting in a large improvement in the PLL performance. This improvement enables accurate estimation of Doppler frequency of extremely weak and high-dynamic signals.

2 Realization of novel phase detector

2.1 The structure of Costas PLL

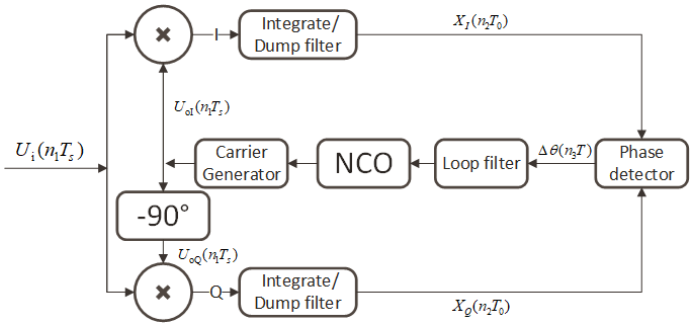

Figure 1. Costas PLL structure.

Figure 1 shows the structure of the PLL. The input signal and the reconstructed signals of the two branches are respectively mixed, and then, the mixed signals are sent to integrate/dump filter. Integrate/dump filter is a low pass filter. We assume that the period used in integrate/dump filter in figure 1 is $T0$, and the function is summing up the data for each continuous period of time($T0$). The phase difference between the real and the reconstructed signals can be identified by phase detector. The phase detector's output is used as the input of the loop filter (LPF). NCO is an integrator. Finally, the NCO's output is used to generate the reconstructed signal.

Figure 2 shows the linear discrete structure of a third-order Costas PLL. The transformation between a continuous system and a discrete system is given by

$$\frac{1}{s} = \frac{Tz^{-1}}{1 - z^{-1}}. \tag{1}$$

The measured Doppler frequency is

$$f_1 = \frac{w_1}{2\pi T}. \tag{2}$$

As is seen in figure 2, loop filter is JR(Jaffe-Rechtin) filter(Tian et al., 2016), w_1 is the output of JR filter. T is sampling period of input data of JR filter. ω_n is natural frequency of PLL.

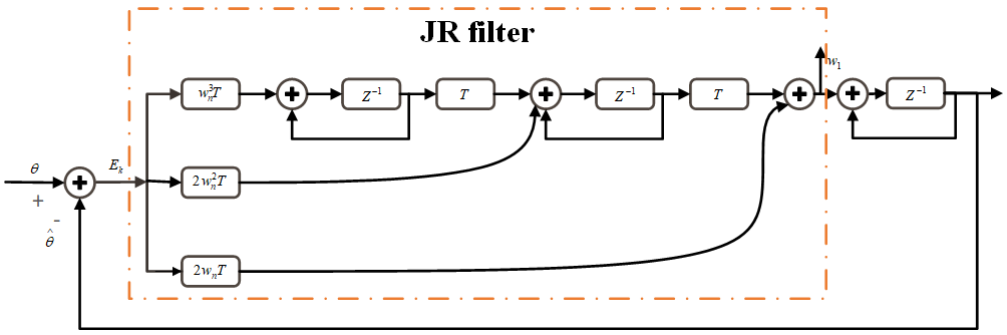

Figure 2. Linear discrete structure of third-order Costas PLL.

2.2 Basic principle of novel phase detector

Wavelet transform is suitable for signal denoising by decomposing signal and noise into different spaces. In the field of optics, wavelet transform can be used for phase retrieval from fringe pattern(Zhong & Weng, 2005). Similar to wavelet function used in wavelet transform, a new basis function is defined and which is given by

$$\psi(t) = (\frac{1}{R} - \frac{t^2}{R^2})exp(-\frac{t^2}{2R^2}) \tag{3}$$

In equation (3), R is an adjustable parameter. In a practical application, R would be set to a fixed constant.

When$R = 1$, $\psi(t)$ is known as Mexican hat wavelet, and the admissibility condition is satisfied. When $R \neq 1$, the admissibility condition is not satisfied, that is, the $\psi(t)$ does not satisfy

$$C_\psi = \int_{-\infty}^{\infty} \frac{|\widehat{\psi}(\omega)|^2}{|w|} d\omega < +\infty \tag{4}$$

$\widehat{\psi}(\omega)$ is Fourier transform of $\psi(t)$. It means that when $R \neq 1$, $\psi(t)$ isn't a wavelet function because the traditional definition of wavelet requires that it satisfies the admissibility condition. But $\psi(t)$ can be still a basis function used in signal transformation.

The Fourier transform of equation (3) is

$$\widehat{\psi}(\omega) = \sqrt{2\pi}(1 - R + R^3\omega^2)exp(-\frac{1}{2}R^2\omega^2). \tag{5}$$

$\widehat{\psi}(\omega)$ is shown in Figure 3. When the frequency exceeds a certain range, the amplitude rapidly decays to close to 0.

Just like family of wavelets defined in wavelet analysis, the corresponding family of $\psi(t)$ is

$$\psi_{a,b}(t) = \frac{1}{\sqrt{a}}\psi(\frac{t-b}{a}). \tag{6}$$

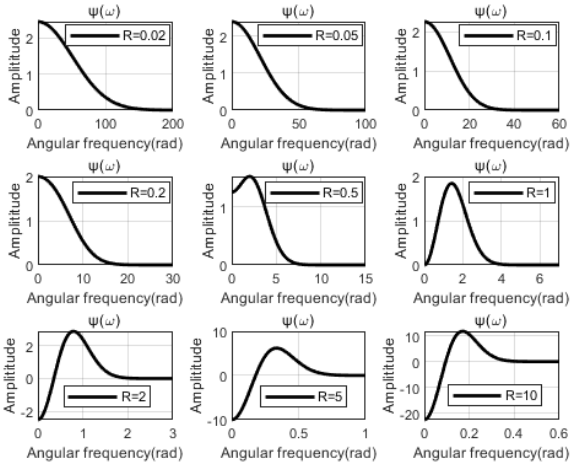

Figure 3. Spectrum of $\psi(t)$ with different R value.

The I way mixed signal is

$$X_I(t) = Acos(2\pi f_0 t + \varphi(t)), t \geq 0. \tag{7}$$

The Taylor expansion of $\varphi(t)$ at $t = b$ is

$$\varphi(t) = \varphi(b) + \varphi'(b)(t-b) + \cdots . \tag{8}$$

If the higher-order terms are ignored, $\varphi(t)$ in the neighborhood of $t = b$ can be expressed as $\varphi(t) = \varphi(b)+\varphi'(b)(t-b)$. Therefore, equation (7) in the neighborhood of $t = b$ is expressed as

$$X_I(t) = Acos(2\pi f_0 t + \varphi(b) + \varphi'(b)(t-b)), t \in (b-\varepsilon, b+\varepsilon). \tag{9}$$

The Fourier transform of equation (9) is

$$\begin{aligned} \widehat{X}_I(w) = {} & A\pi\delta(\varphi'(b) + 2f_0\pi - w)exp(-ib\varphi'(b) + i\varphi(b)) \\ & + A\pi\delta(\varphi'(b) + 2f_0\pi + w)exp(ib\varphi'(b) - i\varphi(b)). \end{aligned} \tag{10}$$

The signal transformation of equation (9) is

$$\begin{aligned} W_{If}(a,b) &= \int_{-\infty}^{\infty} X_I(t)\overline{\psi_{a,b}(t)}dt = \frac{1}{2\pi}\int_{-\infty}^{\infty} \widehat{X}_I(w)\overline{\widehat{\psi}_{a,b}(\omega)}d\omega \\ &= \frac{1}{2\pi}\int_{-\infty}^{\infty} \widehat{X}_I(w)\overline{\widehat{\psi}(a\omega)e^{ib\omega}}d\omega = B(a,b)cos(\varphi(b) + 2bf_0\pi). \end{aligned} \tag{11}$$

In equation (11) $B(a,b) = \sqrt{2\pi}A(1-R+a^2(\varphi'(b)+2f_0\pi)^2)R^3)exp(-\frac{1}{2}a^2(\varphi'(b)+2f_0\pi)^2R^2)$ and overbar " $-$ " denotes a complex conjugation. $W_{If}(a,b)$ is the projection coefficients of $X_I(t)$ on $\psi_{a,b}(t)$.

Similarly, for the Q way mixed signal

$$X_Q(t) = Asin(2\pi f_0 t + \varphi(t)), t \geq 0. \tag{12}$$

The signal transformation of $X_Q(t)$ is

$$W_{Qf}(a,b) = B(a,b)sin(\varphi(b) + 2bf_0\pi). \tag{13}$$

$B(a,b)$ in equation (13) is the same with $B(a,b)$ in equation (11).

The complex variable is constructed by using equations (11) and (13):

$$Z_f(a,b) = W_{If}(a,b) + iW_{Qf}(a,b). \tag{14}$$

When a is determined, $Z_f(a,b)$ degenerates into a complex variable $Z_f(b)$ that is only related to the parameter b. Then, $\varphi(b)$ is expressed as

$$\varphi(b) = arg(Z_f(b)) + 2bf_0\pi. \tag{15}$$

In this study, center frequency $f_0 = 0Hz$. Thus, equation (15) can be simplified to

$$\varphi(b) = arg(Z_f(b)). \tag{16}$$

b is the translation parameter. If a series of time values are taken for b, the phase difference between the real and the reconstructed signals at each time can be obtained. The appropriate value of R in equation (3) is important. As shown in figure 3, the R value determines the spectral characteristics of the basis function. In our application, the spectrum of the basis function should be characteristic of a low pass filter. Therefore, R should be between $0 < R < 1$, with a bias towards small values.

From equation (6), it can be seen that the scale parameter a affects the scaling of the spectrum of $\psi_{a,b}(t)$, and the translation parameter b affects the shift of the spectrum of $\psi_{a,b}(t)$.

Since the duration of the data used in each signal transformation is no more than 0.01 seconds, it means that $b \leq 0.01$. Therefore, the influence of b on the spectrum of $\psi_{a,b}(t)$ can be ignored. Thus, the spectrum of $\psi_{a,b}(t)$ is mainly determined by a and R. For example, when $R = 0.02$ and $a = 50$ are selected, the spectrum of $\psi_{a,b}(t)$ is characteristic of a low pass filter and also has an appropriate cut-off frequency. In fact, there are many other combinations of R and a that can also meet the application requirements, and parameters can be selected according to the characteristics of the actual signal.

In short, we define a new function family $\psi_{a,b}(t)$, then project two signals $X_I(t)$ and $X_Q(t)$ onto $\psi_{a,b}(t)$. When a is a fixed value, the phase can be reconstructed by the projection coefficients of these two signals. The process of signal projection is essentially a signal filtering process, that's the reason why this algorithm proposed here is feasible.

2.3 Data preprocessing by wavelet soft threshold denoising

In practice, the mixed signals $X_I(t)$ and $X_Q(t)$ still contain a lot of noise after being processed by integrate/dump filter. Therefore, if the mixed signal is processed by signal transformation directly, the obtained phase is inaccurate. Therefore, the data preprocessing part must be included in the novel phase discrimination module. Wavelet soft threshold denoising is used in data preprocessing. The discrete Meyer wavelet (Dmey) is selected in this study. The level of wavelet decomposition $n = [log_2 N] - 1$, N is the number of data points which are used in each wavelet transform. $[log_2 N]$ represents taking the integer portion of $log_2 N$. Then, the preprocessed data can be processed by phase discrimination based on signal transformation.

In the process of obtaining the phase of signal when using novel phase discriminator, two steps are included. The first step is preprocessing. Given the frequency of signal is small, a large amount of noise is eliminated by soft threshold denoising. The second step is to use new defined basis function to carry out signal transformation, because the selected basis function is characteristic of a low pass filter, so the noise is also removed in the process of phase extraction by signal transformation. Using an arctangent phase detector to calculate

the phase of signal with a duration of T is to directly calculate the argument angle of the accumulated value of the data in that period. Compared with arctangent phase detector, new phase detector optimizes signal denoising process.

3 Simulation

3.1 Verify correctness of novel phase detector

The two signals are respectively expressed as $X_I(t) = cos(t + 1000t^2)$ and $X_Q(t) = sin(t + 1000t^2)$. This study sets the data sampling rate as $F_s = 4MHz$, time length as $T = 1ms$, and $N = 50$, where N means that the data with a duration of T is evenly divided into N parts according to time and each part is accumulated into 1 point, N is also the number of data points which is used in phase discrimination once. No noise is added.

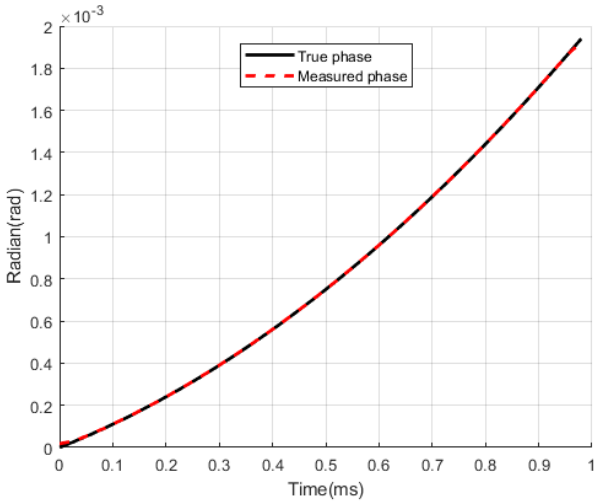

Figure 4. Set $R = 0.02, a = 50$, and the measured phase is shown.

Figure 4 shows that the phase of signal can be reconstructed accurately by using signal transformation based on a new defined basis function. The average phase is obtained by averaging the measured phase, then the average phase is used as the output of novel phase detector and the input of loop filter.

3.2 Validation of performance improvement

In this simulation, a novel phase detector is used to replace arctangent phase detector. The weak signal is expressed as $U_i(t) = cos(2\pi ft) + n_0$, n_0 represents noise. Set 23 sets of signals with different SNR and the signal-to-noise ratios of these signals are respectively $-55dB, -49dB, \cdots, -33dB$. SNR is calculated as $10log_{10}\frac{P_s}{P_n}$, where P_s and P_n are the power of the signal and the noise, respectively. For third-order PLL based on arctangent phase detector and third-order PLL based on novel phase detector, 50 times of carrier tracking experiments were conducted randomly for each group of signals with a set signal-to-noise ratio, and tracking data for 30 seconds at a time. The residual frequency is obtained by subtracting the measured frequency from the true frequency, and root mean square(RMS) is calculated for the residual frequency of last 20 seconds. Frequency of signal is assumed to be locked correctly when RMS$< 1Hz$, thus the probability that the frequency is locked correctly was calculated. In this simulation, sampling rate is $F_s = 4MHz$, the first derivative of the Doppler frequency is $4Hz/s$ and initial frequency is $1MHz$. Make w_n gradually decrease

from 10 to 2 in the first 10 seconds. The time length of the data for phase discrimination once is $T = 10ms$. The scale parameter is $a = 1000$, $R = 0.02$, and $N = 50$. Because $T = NT_0$, then $T_0 = 0.2ms$. The estimated initial frequency is set to $1000002Hz$ in each carrier tracking experiment, so as to eliminate the effect of initial frequency estimation on tracking results.

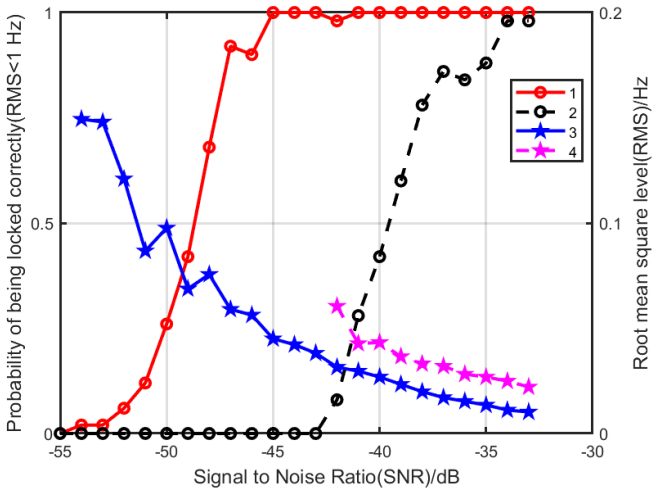

Figure 5. Label 1 and 2 represents Probability of being locked correctly obtained by PLL with novel phase detector and PLL with arctangent phase detector, respectively. Label 3 and 4 represents root mean square level(RMS) of 1 second Integral of residual frequency obtained by PLL with novel phase detector and PLL with arctangent phase detector, respectively. The first derivative of Doppler frequency is 4Hz/s.

As is seen in figure 5, the weak-signal tracking ability of the PLL is greatly improved when arctangent phase detector is replaced by novel phase detector. In addition, the accuracy of Doppler frequency measurement is also significantly improved.

Further, the first derivative of Doppler frequency is set as $100Hz/s$, and make w_n gradually decrease from 20 to 2 in the first 10 seconds. Another simulation result is shown in figure 6. High-dynamic tracking capability and the robustness of PLL algorithm are significantly improved by using novel phase detector.

When using the same hardware, the calculation amount of the two algorithms is compared in Table 1. In simulation, we set sampling rate $F_s = 4MHz$, the duration of data is 1 second and $N = 50$. N is the number of data points which are used in each signal transformation and calculation amount is positive correlated with N. But in our application, $N = 50$ is a proper value, so let N be constant.

In addition, T is a flexible parameter, and the value of T affects the dynamic tracking capability and weak signal tracking capability of PLL. When different values are taken for T, the comparisons between the two PLL algorithms are similar to the results shown in Figure 5 and Figure 6. Table 1 shows the calculation amount of the two kinds of PLL when different values are taken for T. For data of every second , the number of phase discriminations is $1/T$. The smaller the T is, the more phase discriminations are required per second, and the computation is also larger. The new algorithm is currently running in MATLAB, if the code is rewritten by C programming language or some other programming language, then computing time will be decrease significantly.

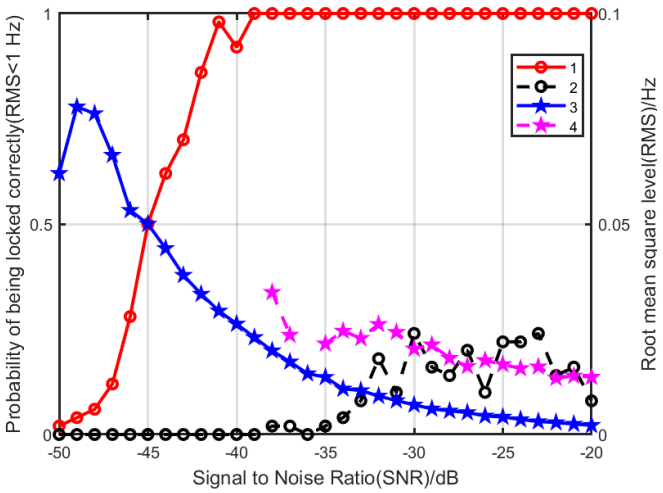

Figure 6. Label 1 and 2 represents Probability of being locked correctly obtained by PLL with novel phase detector and PLL with arctangent phase detector, respectively. Label 3 and 4 represents root mean square level(RMS) of 1 second Integral of residual frequency obtained by PLL with novel phase detector and PLL with arctangent phase detector, respectively. The first derivative of Doppler frequency is 100Hz/s.

Table 1. The amount of computation for both algorithms

Algorithm type	$T = 10ms$ computing time [s]	$T = 5ms$ computing time [s]	$T = 2ms$ computing time [s]	$T = 1ms$ computing time [s]
PLL with arctangent phase detector	0.81	0.78	0.78	0.80
PLL with novel phase detector	1.97	3.04	6.26	11.62

3.3 High-dynamic and extremely weak signal processing

Consider carrier tracking in the entry, descent, and landing (EDL) phase of Mars prober is most challenging. So large dynamic is set in simulation data, figure 7 shows Doppler shift and the first derivative of Doppler shift of simulation data. The maximum second derivative of Doppler shift is $540Hz/s^2$, and the maximum first derivative of Doppler shift is $3612.1Hz/s$. The sampling rate of simulation data is 4MHz, the signal-to-noise ratio(SNR) is set to $-40dB$. T is 2.5ms. The loop noise bandwidth is set to $16.67Hz(w_n = 20)$. Other settings are the same as above.

Most of the signal is drowned out by noise, including the first second data. Therefore, the strategy for rough estimation of initial frequency is to compensate a series of phase values for the first second data and then the frequency index corresponding to maximum amplitude is detected. The obtained frequency index can be used for initialization of PLL.

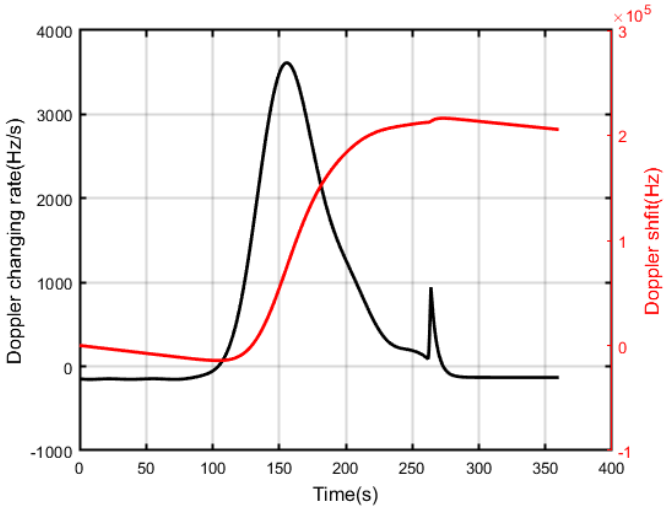

Figure 7. The Doppler shift and Doppler changing rate of simulation data.

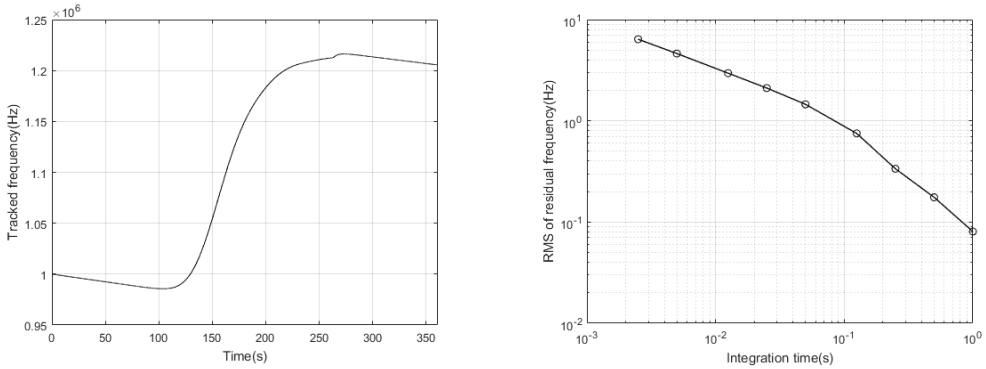

Figure 8. (a) The recovered frequency of simulation data; (b) Tracking accuracy of Doppler frequency at different integration times.

4 Actual data processing

When processing actual data, the loop noise bandwidth is set to $8.33Hz(w_n = 10)$. Actual data consists of four channels of signals which received by UR telescope during the Chang'e-3 landing phase. Figure 9 shows that the actual data processing results also demonstrated the excellent performance of new method and this method will be very useful in deep space exploration.

5 Conclusion

This study proposes a novel phase detector to replace the arctangent phase detector. The new phase discriminator greatly improves performance of PLL, including the weak-signal tracking ability, tracking accuracy and high-dynamic tracking capability. The simulation and actual data processing results demonstrate the effectiveness of this new proposed method.

Data preprocessing in the new phase detector is very important. Data preprocessing can effectively remove noise, an indispensable part of the whole new phase detector.

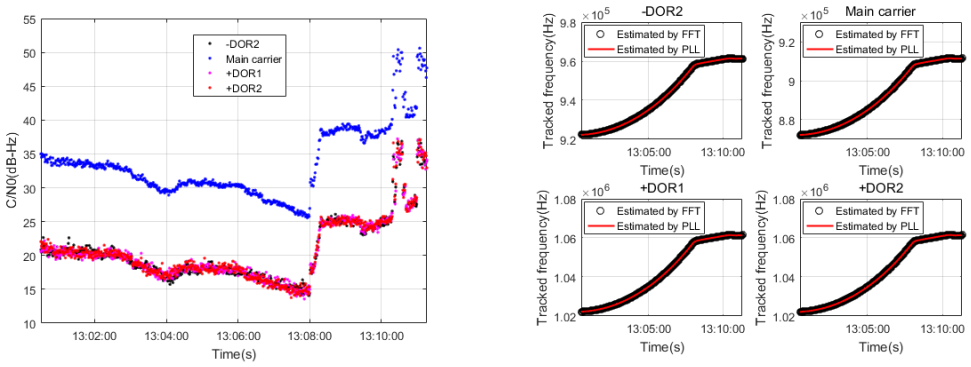

Figure 9. (a) Estimation of the carrier-to-noise ratio of data received by UR telescope during the Chang'e-3 landing phase; (b) The recovered frequency of actual data.

When proper R and a values are selected, the spectrum of $\psi_{a,b}(t)$ should be characteristic of a low pass filter and also has an appropriate cut-off frequency.

There are two reasons not to use traditional wavelets. First, because admissibility condition should be satisfied, the spectrum of wavelets always have the characteristics of a band-pass filter, not a low-pass filter. Second, the phase of the signal may not be obtained by using the coefficients of wavelet transform.

The correct phase detection range of the new phase detector is $\pm\pi$. The reconstructed phase needs to remove the phase value of an integer multiple of 2π to ensure that the phase difference between the real and the reconstructed signals does not exceed the phase discrimination range of the new phase detector. In this way, the divergence of the phase discrimination error can be limited.

Acknowledgments

The present study is supported by the National Natural Science Foundation of China (Grant Nos. 11773060, 11973074, U1831137, and 11703070), National Key Basic Research and Development Program (Grant No. 2018YFA0404702), Shanghai Key Laboratory of Space Navigation and Positioning (Grant No. 3912DZ227330001), and the Key Laboratory for Radio Astronomy of CAS. Data of Change-3 for this research are not publicly available and stored in very long baseline interferometry(VLBI) data processing center of Chinese Academy of Sciences in Shanghai. If someone needs any data of this article, please contact the author via email:dengtao@shao.ac.cn.

References

Cattivelli, F. S., Estabrook, P., Satorius, E. H., & Sayed, A. H. (2008). Carrier recovery enhancement for maximum-likelihood doppler shift estimation in mars exploration missions. *IEEE Journal of Selected Topics in Signal Processing*, *2*(5), 658-669.

Hao, W., Dong, G., Li, H., Wang, H., Fan, M., Zhou, h., & Xu, D. (2018). Key technologies for communications in mars entry descent and landing. *Journal of Deep Space Exploration*, 426-434.

Li, Y., Xu, X., & Zhang, T. (2011). Improving tracking performance of pll based on wavelet packet de-noising technology. In S. Lin & X. Huang (Eds.), *Advances in computer science, environment, ecoinformatics, and education* (pp. 449–456). Berlin, Heidelberg: Springer Berlin Heidelberg.

Lopes, C. G., Satorius, E., & Sayed, A. H. (2006). Adaptive carrier tracking for direct-to-

earth mars communications. In *2006 fortieth asilomar conference on signals, systems and computers* (p. 1042-1046).

Mao, w.-l., & Chen, A.-B. (2008, 03). Mobile gps carrier phase tracking using a novel intelligent dual-loop receiver. *Int. J. Satellite Communications Networking*, *26*, 119-139. doi: 10.1002/sat.898

Pengyue, S., Xiaomei, T., Yangbo, H., Huaming, C., & Guangfu, S. (2016). Adaptive wavelet denoising unscented kalman filter for beidou signal carrier tracking under ionospheric scintillation conditions. *Journal of Applied Remote Sensing*, *10*(4).

Ruan, H., Zhang, L., Luo, Y., & Long, T. (2017). Gnss carrier phase tracking with discrete wavelet transform filtering under ionospheric scintillation. *IEEE Communications Letters*, *21*(2), 394-397.

Satorius, E., Estabrook, P., Wilson, J., & Fort, D. (2003, 01). Direct-to-earth communications and signal processing for mars exploration rover entry, descent, and landing. *Interplanetary Network Progress Report*, 1-.

Soriano, M., Finley, S., Jongeling, A., Fort, D., Goodhart, C., Rogstad, D., & Navarro, R. (2012, 03). Spacecraft-to-earth communications for juno and mars science laboratory critical events.
doi: 10.1109/AERO.2012.6187098

Sun, P., Tang, X., Huang, Y., & Sun, G. (2017). Wavelet de-noising kalman filter-based global navigation satellite system carrier tracking in the presence of ionospheric scintillation. *IET Radar, Sonar Navigation*, *11*(2), 226-234.

Tian, T., Cui, C., & Cheng, L. (2016). Design and simulation of third order phase-locked loop in high-dynamic applications. *Space Electronic Technology*, *13*(4), 57-60.

Vil-Valls, J., Closas, P., & Fernndez-Prades, C. (2015). On the identifiability of noise statistics and adaptive kf design for robust gnss carrier tracking. In *2015 ieee aerospace conference* (p. 1-10).

Vila-Valls, J., Closas, P., Navarro, M., & Fernandez-Prades, C. (2017). Are plls dead? a tutorial on kalman filter-based techniques for digital carrier synchronization. *IEEE Aerospace and Electronic Systems Magazine*, *32*(7), 28-45.

Won, J. (2014). A novel adaptive digital phase-lock-loop for modern digital gnss receivers. *IEEE Communications Letters*, *18*(1), 46-49.

Won, J., Pany, T., & Eissfeller, B. (2012). Characteristics of kalman filters for gnss signal tracking loop. *IEEE Transactions on Aerospace and Electronic Systems*, *48*(4), 3671-3681.

Zhong, J., & Weng, J. (2005, Oct). Phase retrieval of optical fringe patterns from the ridge of a wavelet transform. *Opt. Lett.*, *30*(19), 2560–2562. Retrieved from `http://ol.osa.org/abstract.cfm?URI=ol-30-19-2560` doi: 10.1364/OL.30.002560